



Phase-space path-integral representation of the quantum density of states: Monte Carlo simulation of strongly correlated soft-sphere fermions

V. S. Filinov , P. R. Levashov , and A. S. Larkin

Joint Institute for High Temperatures RAS, Izhorskaya 13 Building 2, Moscow 125412, Russia



(Received 31 October 2023; accepted 30 January 2024; published 27 February 2024)

The Wigner formulation of quantum mechanics is used to derive a path-integral representation of the quantum density of states (DOS) of strongly correlated fermions in the canonical ensemble. A path-integral Monte Carlo approach for the simulation of DOS and other thermodynamic functions is suggested. The derived Wigner function in the phase space resembles the Maxwell-Boltzmann distribution but allows for quantum effects. We consider a three-dimensional quantum system of strongly correlated soft-sphere fermions at different densities and temperatures. The calculated properties include the DOS, momentum distribution functions, spin-resolved radial distribution functions, potentials of mean force, and related energy levels obtained from the Bohr-Sommerfeld condition. We observe sharp peaks on DOS and momentum distribution curves, which are explained by the appearance of fermionic bound states.

DOI: [10.1103/PhysRevE.109.024137](https://doi.org/10.1103/PhysRevE.109.024137)

I. INTRODUCTION

Density of states (DOS) is one of the fundamental concepts of statistical physics. The DOS $\Omega(E)$ is defined as the number of states in the range from E to $E + \delta E$ per unit volume. This function can be used to compute all thermodynamic properties of a system and is highly relevant for the study of a wide variety of systems, including strongly coupled systems of particles with a rough energy landscape. The DOS permits us to directly compute the free energy and entropy and is instrumental for the study of phase transitions.

Due to the importance of DOS, many works are devoted to the calculation of this quantity using, in particular, generalized ensembles and reweighting techniques [1–3]. The most prominent approach is the Wang-Landau (WL) algorithm, which is a Monte Carlo technique for computing the DOS of classical and quantum systems [4–11]. DOS can be directly calculated in density functional theory (DFT) [12] and therefore the DOS analysis is widely used in solid-state and condensed-matter physics [13,14]. However, DFT cannot be applied for some systems or leads to a severe computational workload [15].

Attempts to develop fast and accurate methods for calculating DOS and thermodynamic functions have been repeatedly made [16–18]. An interesting approach involving path integrals was suggested in the article [19], in which the entropic sampling [20] was applied within the Wang-Landau algorithm to calculate the DOS for a three-dimensional (3D) quantum system of harmonic oscillators at a finite temperature. In the path-integral formalism quantum particles are presented as “trajectories” in the configuration space or “ring polymers” consisting of a lot of “beads” connected by harmonic-like bonds (springs) [19]. As a result, the exact data for the energy and canonical distribution were reproduced for a wide range of temperatures.

The main disadvantage of the path-integral Monte Carlo method (PIMC) for simulations of Fermi systems is the

“fermionic sign problem” arising due to the antisymmetrization of a fermion density matrix [21] and resulting in thermodynamic quantities being small differences of large numbers associated with even and odd permutations. As a consequence, the statistical error in PIMC simulations grows exponentially with the number of particles. To overcome this issue many approaches were developed [22–26]. In Refs. [27,28] to avoid the “fermionic sign problem,” a restricted fixed-node path-integral Monte Carlo (RPIMC) approach was offered. In RPIMC only positive permutations are taken into account and the accuracy of the results depends on the conformation of the nodal surface.

An alternative approach based on the Wigner formulation of quantum mechanics in the phase space [29,30] was used in Refs. [31,32] to avoid the antisymmetrization of matrix elements and hence the “sign problem.” This approach allows us to reproduce the Pauli blocking of fermions and is able to calculate quantum momentum distribution functions as well as transport properties [23]. Average values of quantum operators in the phase space are also available. However, the approach is not applicable at high degeneracy. Thus, the “fermionic sign problem” for strongly correlated fermions has not been completely solved since the early 1970s.

In this paper we continue developing the phase-space path-integral technique by applying it to the DOS of a strongly coupled soft-sphere fermions. The developed DOS approximation is antisymmetrized and is more accurate and rigorous in comparison with the previous ones [31–33]. Let us stress that the Wigner approach to quantum mechanics can incorporate two semiclassical concepts: the Bohr-Sommerfeld quantization condition and the Heisenberg correspondence principle for obtaining approximate matrix elements of any operator (see the recently developed symmetrical quasiclassical Meyer-Miller approach [34–36]). In our paper we develop a PIMC method based on the Wigner approach (WPIMC) being a compromise between the accuracy and speed of simulations.

A simple model of 3D soft-sphere fermions is well known in statistical physics and was chosen to demonstrate the correctness of our method. This model includes the one-component plasma, which is of great astrophysical importance [37,38]. Moreover, the theoretical studies of strongly interacting particles obeying the Fermi-Dirac statistics is the subject of general interest in many fields of physics, in particular, plasma under extreme conditions [23], uniform electron gas [39], quantum liquids such as ^3He [40], and so on. The suggested approach is applicable for predicting DOS not only for bulk structures (3D) but also for surfaces (2D) in multicomponent systems.

In Sec. II we consider a path-integral description of quantum DOS in the Wigner formulation of quantum mechanics. In Sec. III we present the results of our simulations by the WPIMC method for a 3D quantum system of strongly correlated soft-sphere fermions. DOS, momentum distribution functions, spin-resolved radial distribution functions, potentials of mean force, and related energy levels obtained from the Bohr-Sommerfeld condition are calculated. In Sec. IV we summarize the obtained properties and discuss their physical meaning. The derivation of the quantum effective interparticle interaction as well as the details of the WPIMC method are given in Appendixes A and B.

II. PATH-INTEGRAL REPRESENTATION OF THE DENSITY OF STATES

The DOS is a fundamental function of a system and can be used to compute important thermodynamic properties such as, for example, internal energy, entropy, and heat capacity. It can be defined as $\Omega(E) = \text{Tr}\{\delta(E\hat{I} - \hat{H})\}$ [41], where \hat{I} is the unit operator and \hat{H} is the Hamiltonian of the system, while δ is the delta function. The expression $\Omega(E)dE$ determines the number of states between E and $E + dE$ per unit volume [42].

The Hamiltonian of the system $\hat{H} = \hat{K} + \hat{U}$ contains the kinetic energy \hat{K} and the potential energy \hat{U} taken as the sum of pair interactions $\phi(r) = \epsilon(\sigma/r)^n$, where r is the interparticle distance, σ characterizes the effective particle size, ϵ sets the energy scale, and n determines the potential hardness. As an example, we consider the parameters $\epsilon/k_B \simeq 27K$ (k_B is the Boltzmann constant) and $\sigma = 2.71 \text{ \AA}$ used to described quantum helium-3 in the canonical ensemble [43].

The useful identical form of $\Omega(E)$ is

$$\begin{aligned} \Omega(E) &= \text{Tr}\{\delta(E\hat{I} - \hat{H})\hat{I}\} = \text{Tr}\{\delta(E\hat{I} - \hat{H})e^{(E\hat{I} - \hat{H})}\} \\ &= \frac{1}{2\pi} \int d\omega \text{Tr}\{e^{i\omega(E\hat{I} - \hat{H})} e^{(E\hat{I} - \hat{H})}\} \\ &= \frac{1}{2\pi} \int d\omega \text{Tr}\{e^{\kappa(\omega)(E\hat{I} - \hat{H})}\} \\ &= \frac{1}{2\pi} \int d\omega \int dq_1 \langle q_1 | e^{\kappa(\omega)(E\hat{I} - \hat{H})} | q_1 \rangle, \end{aligned} \quad (1)$$

where $\kappa(\omega) = 1 + i\omega$, angular brackets $\langle q | \tilde{q} \rangle$ denote the scalar product of the eigenvectors $|q\rangle$ and $|\tilde{q}\rangle$ of the position operator \hat{q} [30], the angular brackets in the expression $\langle q_1 | \hat{A} | q \rangle$ denote the scalar product of vectors $|q_1\rangle$ and $|\hat{A}|q\rangle$, and i is the imaginary unit. Henceforth it is convenient to imply that energy is expressed in units of $k_B T$ (T is the

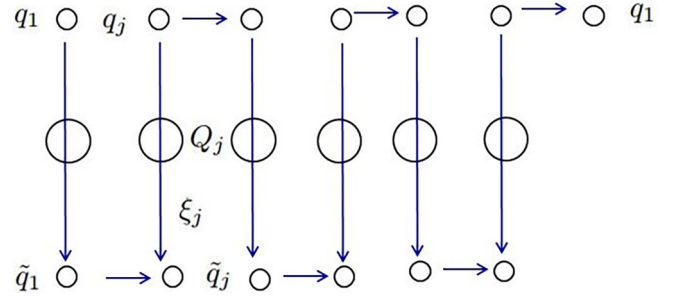


FIG. 1. The symbolic representation of the DOS by Eq. (2), where the “vertical” $\langle q_j | \exp \frac{i\omega}{M}(E\hat{I} - \hat{H}) | \tilde{q}_j \rangle$ and “horizontal” $\langle q_j | \exp \frac{1}{M}(E\hat{I} - \hat{H}) | q_{j+1} \rangle$ ($\langle \tilde{q}_j | \exp \frac{1}{M}(E\hat{I} - \hat{H}) | \tilde{q}_{j+1} \rangle$) matrix elements are shown by the related arrows.

temperature of the system) and q_1 is a $3N$ -dimensional vector of the particle positions.

The main difficulty is that the operators of kinetic and potential energy do not commute and, as a consequence, an exact explicit analytical expression for the DOS is unknown. Nevertheless, it can be constructed using a path-integral approach [21,22,44] based on the semigroup property $\exp(\kappa(\omega)(E\hat{I} - \hat{H})) = \exp(\epsilon(\omega)(E\hat{I} - \hat{H})) \times \dots \times \exp(\epsilon(\omega)(E\hat{I} - \hat{H}))$ with $\epsilon(\omega) = \kappa(\omega)/M$ (M is a large positive integer), so that

$$\begin{aligned} \Omega(E) &= \frac{1}{2\pi} \int d\omega \int dq_1 \langle q_1 | e^{\kappa(\omega)(E\hat{I} - \hat{H})} | q_1 \rangle \\ &= \frac{1}{2\pi} \int d\omega \prod_{j=1}^M \int dq_j d\tilde{q}_j \\ &\quad \times \langle q_1 | e^{i\omega(E\hat{I} - \hat{H})/M} | \tilde{q}_1 \rangle \langle \tilde{q}_1 | e^{(E\hat{I} - \hat{H})/M} | \tilde{q}_2 \rangle \\ &\quad \times \langle \tilde{q}_2 | e^{i\omega(E\hat{I} - \hat{H})/M} | q_2 \rangle \langle q_2 | e^{(E\hat{I} - \hat{H})/M} | q_3 \rangle \\ &\quad \times \langle q_3 | e^{i\omega(E\hat{I} - \hat{H})/M} | \tilde{q}_3 \rangle \langle \tilde{q}_3 | e^{(E\hat{I} - \hat{H})/M} | \tilde{q}_4 \rangle \dots \\ &\quad \times \langle \tilde{q}_M | e^{i\omega(E\hat{I} - \hat{H})/M} | q_M \rangle \langle q_M | e^{(E\hat{I} - \hat{H})/M} | q_1 \rangle, \end{aligned} \quad (2)$$

where we used the position representation of the operators. In order to understand Eq. (2) its mathematical structure is shown in Fig. 1 in a symbolic form. Here the variables Q_j and ξ_j are defined as $Q_j = (\tilde{q}_j + q_j)/2$, $\xi_j = (\tilde{q}_j - q_j)$ for $j = 1, \dots, M$ ($q_j = Q_j - \xi_j/2$, and $\tilde{q}_j = Q_j + \xi_j/2$). Further, for convenience we will use both set of variables (Q, ξ) and (q, \tilde{q}) .

The Weyl symbol of the operator \hat{H} is the Hamiltonian function $H(p, q)$ defined as [29,30]

$$H(p, q) = \int d\xi \exp(i\langle p | \xi \rangle) \langle q - \xi/2 | \hat{H} | q + \xi/2 \rangle, \quad (3)$$

where ξ and p are $3N$ -dimensional vectors. The inverse Fourier transform allows us to express the matrix elements of an operator through their Weyl symbols. So for large M with the error of the order of $(1/M)^2$ required for the path-integral

approach [21,22] we have

$$\begin{aligned}
& \langle Q_j - \xi_j/2 | \exp \frac{i\omega}{M} (E\hat{I} - \hat{H}) | Q_j + \xi_j/2 \rangle \\
& \approx \langle Q_j - \xi_j/2 | \hat{I} + \frac{i\omega}{M} (E\hat{I} - \hat{H}) | Q_j + \xi_j/2 \rangle + O\left(\frac{1}{M^2}\right) \\
& = \left(\frac{1}{2\pi}\right)^{3N} \int dP_j e^{-i\langle P_j | \xi_j \rangle} \left\{ 1 + \frac{i\omega}{M} [E - H(P_j, Q_j)] \right\} \\
& \approx \left(\frac{1}{2\pi}\right)^{3N} \int dP_j e^{-i\langle P_j | \xi_j \rangle} e^{i\omega [E - H(P_j, Q_j)]/M} + O\left(\frac{1}{M^2}\right), \quad (4)
\end{aligned}$$

where $H(P_j, Q_j) = \langle P_j | P_j \rangle / 2m + U(Q_j)$ are the sums of the Hamilton functions for N particles at a given j .

The final expression for the product is

$$\begin{aligned}
& \prod_{j=1}^M \langle q_j | \exp \frac{i\omega}{M} (E\hat{I} - \hat{H}) | \tilde{q}_j \rangle \approx \left(\frac{1}{2\pi}\right)^{3NM} \\
& \times \prod_{j=1}^M \int dP_j \exp(-i\langle P_j | \xi_j \rangle) \exp \frac{i\omega}{M} [E - H(P_j, Q_j)]. \quad (5)
\end{aligned}$$

This is the operator analog of the $\lim_{M \rightarrow \infty} (1 + x/M)^M = (e^{x/M})^M$.

Then the DOS is presented as

$$\begin{aligned}
\Omega(E) &= \left(\frac{1}{2\pi}\right)^{3NM+1} \int dQ dP \int d\omega e^{i\omega [E - H(P, Q)]} \int d\xi e^{-i\langle P | \xi \rangle} \\
& \times \langle \tilde{q}_1 | e^{(E\hat{I} - \hat{H})/M} | \tilde{q}_2 \rangle \langle q_2 | e^{(E\hat{I} - \hat{H})/M} | q_3 \rangle \\
& \times \langle \tilde{q}_3 | e^{(E\hat{I} - \hat{H})/M} | \tilde{q}_4 \rangle \dots \langle q_M | e^{(E\hat{I} - \hat{H})/M} | q_1 \rangle, \quad (6)
\end{aligned}$$

where only ‘‘horizontal’’ matrix elements remained (see Fig. 1), $H(P, Q) = \sum_{j=1}^M H(P_j, Q_j)/M$, $Q = \{Q_1, \dots, Q_M\}$, and $P = \{P_1, \dots, P_M\}$, $\xi = \{\xi_1, \dots, \xi_M\}$ are $3NM$ -dimensional vectors and $\prod_{j=1}^M dq_j d\tilde{q}_j = dQ d\xi$.

The final expression for the DOS in the Wigner representation can be written as

$$\Omega(E) = \exp(E) \int dQ dP \delta[E - H(P, Q)] W(P, Q), \quad (7)$$

where $\delta[E - H(P, Q)]$ is the path-integral analog of the Weyl symbol of the operator $\delta(E\hat{I} - \hat{H})$ [29,30],

$$\begin{aligned}
\delta[E - H(P, Q)] &= \frac{1}{2\pi} \int d\omega e^{i\omega (E - H(P, Q))} \\
&\approx \frac{1}{2\pi} \int d\omega e^{i\omega \langle P | \xi \rangle} \prod_{j=1}^M \langle q_j | e^{i\omega (E\hat{I} - \hat{H})/M} | \tilde{q}_j \rangle, \quad (8)
\end{aligned}$$

and the generalization of the Wigner function $W(P, Q)$ can be defined as

$$\begin{aligned}
W(P, Q) &= \left(\frac{1}{2\pi}\right)^{3NM} e^{-E} \int d\xi e^{-i\langle P | \xi \rangle} \\
& \times \langle \tilde{q}_1 | e^{(E\hat{I} - \hat{H})/M} | \tilde{q}_2 \rangle \langle q_2 | e^{(E\hat{I} - \hat{H})/M} | q_3 \rangle \dots \\
& \times \langle q_M | e^{(E\hat{I} - \hat{H})/M} | q_1 \rangle. \quad (9)
\end{aligned}$$

Herein we assume that the operator \hat{H} does not depend on the spin variables. However, the spin variables σ and the Fermi statistics can be taken into account by the following redefinition of $W(P, Q)$ in the canonical ensemble with temperature T :

$$\begin{aligned}
W(P, Q) &= \frac{1}{Z(\beta)N!} \exp(-E) \sum_{\sigma} \sum_{\mathcal{P}} (-1)^{\kappa_{\mathcal{P}}} \mathcal{S}(\sigma, \mathcal{P}\sigma') \Big|_{\sigma'=\sigma} \int d\xi \exp(-i\langle P | \xi \rangle) \\
& \times \langle \tilde{q}_1 | \exp \frac{1}{M} (E\hat{I} - \hat{H}) | \tilde{q}_2 \rangle \langle q_2 | \exp \frac{1}{M} (E\hat{I} - \hat{H}) | q_3 \rangle \langle \tilde{q}_3 | \exp \frac{1}{M} (E\hat{I} - \hat{H}) | \tilde{q}_4 \rangle \dots \langle q_M | \exp \frac{1}{M} (E\hat{I} - \hat{H}) | q_1 \rangle \\
& = \frac{1}{Z(\beta)N!} \int d\xi \exp(-i\langle P | \xi \rangle) \rho^{(1)} \dots \rho^{(M-1)} \sum_{\sigma} \sum_{\mathcal{P}} (-1)^{\kappa_{\mathcal{P}}} \mathcal{S}(\sigma, \mathcal{P}\sigma') \Big|_{\sigma'=\sigma} \mathcal{P} \rho^{(M)} \Big|_{q_{(M+1)}=q_1}, \quad (10)
\end{aligned}$$

where the sum is taken over all permutations \mathcal{P} with the parity $\kappa_{\mathcal{P}}$ and index j labels the off-diagonal high-temperature density matrices $\rho^{(j)} \equiv \langle Q_j \pm \xi_j/2 | e^{-\frac{1}{M}\hat{H}} | Q_{j+1} \pm \xi_{j+1}/2 \rangle$. Here, as in expression (6), only the ‘‘horizontal’’ matrix elements are present. With the error of the order of $1/M^2$ each high-temperature factor can be presented in the form $\rho^{(j)} = \langle Q_j \pm \xi_j/2 | e^{-\frac{1}{M}\hat{H}} | Q_{j+1} \pm \xi_{j+1}/2 \rangle \approx e^{-\frac{1}{M}\hat{U}(Q_j \pm \xi_j/2)} \rho_0^{(j)}$ with $\rho_0^{(j)} = \langle Q_j \pm \xi_j/2 | e^{-\frac{1}{M}\hat{K}} | Q_{j+1} \pm \xi_{(j+1)}/2 \rangle$, arising from neglecting the commutator $[K, U]/(2M^2)$ and further terms of the expansion. In the limit $M \rightarrow \infty$ the error of the whole product of high-temperature factors tends to zero ($\propto 1/M$) and we have an exact path-integral representation of the Wigner functions.

We imply that momenta and positions are dimensionless variables $p\tilde{\lambda}/\hbar$ and $q/\tilde{\lambda}$ related to a temperature MT [$\tilde{\lambda} = \sqrt{2\pi\hbar^2\beta/(mM)}$]. Spin gives rise to the standard spin part of the density matrix $\mathcal{S}(\sigma, \mathcal{P}\sigma') = \prod_{k=1}^N \delta(\sigma_k, \sigma_{\mathcal{P}k})$ ($\delta(\sigma_k, \sigma_r)$ is the Kronecker symbol) with exchange effects accounted for by the permutation operator \mathcal{P} acting on coordinates of particles \tilde{q}_{M+1} and spin projections σ' .

In general the complex-valued integral over ξ in the definition of the Wigner function (10) cannot be calculated analytically. Moreover, this integration is inconvenient for Monte Carlo calculation. To overcome this difficulty we have to obtain an explicit expression for $W(P, Q)$. However, analytic integration over ξ is possible only for the linear or

harmonic potentials, when the power of variable ξ is not more than two. For this reason we use an approximation for potential energy U arising, for example, from the Taylor expansion up to the first order with respect to ξ [32,45],

$$U(Q_j \pm \xi_j/2) \approx U(Q_j) \pm \frac{1}{2} \left\langle \xi_j \left| \frac{\partial U(Q_j)}{\partial Q_j} \right. \right\rangle. \quad (11)$$

Here the second term denotes the scalar product of the vector ξ and the multidimensional gradient of pseudopotential energy.

Then let us replace the variables of integration Q_j by ζ_j for any given permutation \mathcal{P} using the substitution [32,45],

$$Q_j = (\tilde{\mathcal{P}}Q_{M+1} - Q_1) \frac{j-1}{M} + Q_1 + \zeta_j, \quad (12)$$

where $\tilde{\mathcal{P}}$ is the matrix representing the permutation operator \mathcal{P} equal to the unit matrix E with appropriately transposed columns. This replacement presents each trajectory Q_j as the sum of the ‘‘straight line’’ $(\tilde{\mathcal{P}}Q_{M+1} - Q_1) \frac{j-1}{M} + Q_1$ and the deviation ζ_j from it for $j = 1, \dots, M+1$ (here $Q_{M+1} = Q_1$, while in a general case $Q_{M+1} \neq Q_1$). As a consequence the matrix elements can be rewritten in the form of a path integral over ‘‘closed’’ trajectories $\{\zeta_1, \dots, \zeta_M\}$ with $\zeta_1 = \zeta_{M+1} = 0$ (‘‘ring polymers’’).

Then after the Hubbard-Stratonovich transformations and some additional ones (including analytical continuation of ϕ and the integration over ξ and x) the main contribution to the Wigner function can be written in the form containing the Maxwell distribution with quantum corrections [46–48],

$$\begin{aligned} W(P, Q) &= \frac{C(M)}{Z(\beta)N!} \sum_{\sigma} \sum_{\mathcal{P}} (\pm 1)^{k_{\mathcal{P}}} \mathcal{S}(\sigma, \mathcal{P}\sigma') \Big|_{\sigma'=\sigma} \int d\xi \exp \left\{ -i \langle \xi | P \rangle - \pi \sum_{j=1}^M \left[|Q_{j+1} - Q_j|^2 + \frac{1}{4} |\xi_{j+1} - \xi_j|^2 \right. \right. \\ &\quad \left. \left. + (-1)^j \left[\langle Q_{j+1} - Q_j | \xi_{j+1} - \xi_j \rangle + \left\langle \xi_j \left| \frac{\partial U_j^{\tilde{\mathcal{P}}}}{2M \partial \zeta_j} \right. \right\rangle \right] \right\} - U_{\mathcal{P}} \Big\} \\ &= \frac{C(M)}{Z(\beta)N!} \sum_{\sigma} \sum_{\mathcal{P}} (\pm 1)^{k_{\mathcal{P}}} \mathcal{S}(\sigma, \mathcal{P}\sigma') \Big|_{\sigma'=\sigma} \times \exp \left\{ -\pi \frac{|\tilde{\mathcal{P}}Q_1 - Q_1|^2}{M} - \sum_{j=1}^M \pi |\eta_j|^2 - U_{\mathcal{P}} \right\} \int dx \exp \left\{ -\sum_{j=1}^M \frac{\langle x_j | x_j \rangle}{2} \right\} \\ &\quad \times \int d\xi \exp \left(-i \langle \xi | P \rangle - i \sum_{j=1}^M \left\{ \left\langle \frac{x_j}{2} + \eta_j \right| (-1)^j [\xi_{j+1} - \xi_j] \right\} - i (-1)^j \left\langle \xi_j \left| \frac{\partial U_j^{\tilde{\mathcal{P}}}}{2M \partial \zeta_j} \right. \right\rangle \right) \\ &\approx \frac{\tilde{C}(M)}{Z(\beta)N!} \exp \left[-\sum_{j=1}^M \pi |\eta_j|^2 - U_{\mathcal{E}} \right] \exp \left\{ \frac{M}{4\pi} \sum_{j=1}^M \langle i \tilde{\mathcal{P}}_j | i \tilde{\mathcal{P}}_j \rangle \right\} \times \det \| \tilde{\phi}^{kt} \|_1^{N/2} \det \| \tilde{\phi}^{kt} \|_{(N/2+1)}^{N_c}, \end{aligned} \quad (13)$$

where $\eta_j \equiv \zeta_{j+1} - \zeta_j$,

$$U_{\mathcal{E}} = \frac{1}{M} \sum_{j=1}^M U_j(Q_1 + \zeta_j),$$

$$U_{\mathcal{P}} = \frac{1}{M} \sum_{j=1}^M U_j^{\tilde{\mathcal{P}}} \left[(\tilde{\mathcal{P}}Q_1 - Q_1) \frac{j-1}{M} + Q_1 + \zeta_j \right],$$

$$\tilde{\phi}^{kt} = \exp \{ -\pi |r_{kt}|^2 / M \} \exp \left\{ -\frac{1}{M} \sum_{j=1}^M \left(\bar{\phi}_j^{kt} - \phi_j^{kt} \right) \right\},$$

$$\bar{\phi}_j^{kt} = \phi \left[\left| r_{tk} \frac{2j}{M} + r_{kt} + (\zeta_j^k - \zeta_j^t) \right| \right],$$

$$\phi_j^{kt} = \phi \left[|r_{kt} + (\zeta_j^k - \zeta_j^t)| \right],$$

$$\tilde{\mathcal{P}}_j \approx P_j - i(-1)^j \frac{1}{2M} \frac{\partial U_j^{\tilde{\mathcal{P}}}}{\partial \zeta_j},$$

and $r_{kt} \equiv (Q_1^k - Q_1^t)$. The partial derivatives have here $3N$ components. The constants $C(M)$ as well as $\tilde{C}(M)$ are canceled in Monte Carlo calculations.

In the thermodynamic limit the main contribution in the sum over spin variables comes from the term related to the equal numbers $N/2$ of fermions with the same spin projection [23,24] and the sum over permutations gives the product of determinants. The partition function Z is canceled in Monte Carlo calculations.

Let us stress that approximation (13) has the correct limits in the cases of weakly and strongly degenerate fermionic systems. Indeed, in the classical limit the main contribution comes from the diagonal matrix elements due to the factor $\exp\{-\pi|r_{kt}|^2/M\}$ and potential energies ($U_{\mathcal{E}}$) in the exponents have to be related to the identical permutation.

At the same time, when the thermal wavelength is of the order of the average interparticle distance and the trajectories are highly entangled the potential energy weakly depends on permutations and can be approximated by the potential energy ($U_{\mathcal{E}}$) related to the identical permutation [47,48].

Thus, the problem is reduced to calculating the matrix elements of the density matrix $\rho = \exp(-\hat{H})$, which is similar to the simulation of thermodynamic properties and, according to Eq. (7), the problem of DOS calculation is reduced to the consideration of the internal-energy histogram in the canonical ensemble multiplied by $\exp(E)$.

III. RESULTS OF SIMULATIONS

Here, as an interesting example, we present the results of the WPIMC calculations of the radial (RDFs) and momentum (MDFs) distribution functions, as well as the DOS for the 3D system of Fermi particles strongly interacting via the soft-sphere potential with hardness $n = 0.2$ and $n = 1.4$. Here the density of soft spheres is characterized by the parameter $r_s = a/\sigma$ defined as the ratio of the mean distance between the particles $a = [3/(4\pi\bar{\rho})]^{1/3}$ to σ ($\bar{\rho}$ is the number density). The results presented below have been obtained for the following physical parameters used in Ref. [43] for PIMC simulations of helium-3: $\epsilon \simeq 27$ K, $\sigma \simeq 5.2 a_B$ (a_B is the Bohr radius), $m_a = 3.016$ is the soft-sphere mass in atomic units.

To calculate these functions by the WPIMC (see Appendix B for details) the Markovian chain of particle configurations were generated using the Metropolis algorithm. We use a standard basic Monte Carlo cell with periodic boundary conditions. Between 10^6 and 3×10^6 equilibrium configurations of 300, 600, and 900 particles represented by 20 and 40 “beads” have been used to calculate average values. The convergence and statistical error of the calculated functions were tested with increasing number of Monte Carlo steps, number of particles and beads at a different hardness of the soft-sphere potential. It turned out that 600 particles represented by 20 beads were enough to reach good convergence.

The RDF [49,50], MDF, internal-energy distribution function and DOS can be written as follows:

$$\begin{aligned} g_{ab}(r) &= \int dP dQ \delta(|Q_1^a - Q_1^b| - r) W(P, Q), \\ W(|P^a|) &= \int d\tilde{P} dQ \delta(|P^a| - |\tilde{P}|) W(\tilde{P}, Q), \\ W(E) &= \int dP dQ \delta(E - H(P, Q)) W(P, Q), \\ \Omega(E) &= \exp(E) W(E), \end{aligned} \quad (14)$$

where a and b label fermions and E and $H(P, Q)$ are energy per particle. The RDF g_{ab} is proportional to the probability density to find a pair of particles of types a and b at a certain distance r from each other. In an isotropic system the RDF depends only on the difference of coordinates because of the translational invariance of the system. In a classical noninteracting system of particles $g_{ab} \equiv 1$, while interaction, quantum effects and statistics result in the spacial redistribution of particles and a nonmonotonic RDF.

The MDF and internal energy are defined by the Maxwell-Boltzmann distribution and interparticle interaction. In 2D and 3D systems the DOS is proportional to $\Omega \sim \text{const}$ and $\Omega \sim \sqrt{E}$, respectively [41].

Figure 2 shows some typical results of the WPIMC simulations. We present the RDFs (g), MDFs [$W(|P|)$], DOS [$\Omega(E)$], the potentials of the mean force [$W^{(2)}(r)$] and estimations of the averaged energy levels (E_L) in the system of strongly coupled fermions.

A. Radial distribution functions

To analyze the conditions of arising the individual separated sharp high peaks on the DOS and MDF curves let

us consider the RDFs. The difference revealed between the RDFs with the same and opposite spin projections of fermions is impressive. At small interparticle distances all RDFs tend to zero due to the repulsion of the soft-sphere potential. An additional contribution to the repulsion of fermions with the same spin projection at distances of the order of the thermal wavelength (lines 2) is caused by the Fermi statistics effect described by the exchange determinant in (13). This additional repulsion leads to the formation of cavities (usually called exchange-correlation holes) for fermions with the same spin projection and results in the formation of high peaks on the corresponding RDFs due to the strong excluded volume effect [51]. The RDFs for fermions with the same spin projection show that the characteristic “size” of an exchange-correlation cavity with corresponding peaks is of the order of the soft-sphere thermal wavelength ($\lambda/\sigma \sim 0.63$, $r_s = 3.77$, and $\lambda/\sigma \sim 1$, $r_s = 6.84$ for temperatures $T = 40$ K and $T = 20$ K, respectively), which is less than the average interparticle distance. Let us stress that the strong excluded volume effect was observed in the classical systems of hard spheres in the early 1970s [52] and was derived analytically for the 1D case in Ref. [50]. For fermions with the opposite spin projections the interparticle interaction is not enough to form any peaks on the RDF. At large interparticle distances the RDFs decay monotonically to unity due to the short-range repulsion of the potential. With increasing density and hardness the height of the peaks is growing.

B. Potentials of mean force, the Bohr-Sommerfeld condition, energy levels, and MDFs

To analyze the conditions of arising the individual separated sharp high peaks on the DOS and MDF curves let us consider RDFs and the corresponding potentials of mean interparticle force. The potentials of mean force (PMF) $W^{(k)}$ [49] of a classical N -particle system is defined up to an arbitrary constant as

$$-\nabla_j W^{(k)} = \frac{\int e^{-\beta U} (-\nabla_j U) dq_{k+1} \dots dq_N}{\int e^{-\beta U} dq_{k+1} \dots dq_N}, \quad (15)$$

where $j = 1, 2, \dots, k$. Here $-\nabla_j W^{(k)}$ is the “mean force” acting on a j th particle at a given position of any k particles. For $k = 2$ $W^{(2)}$ is related to the RDF of the system as $g(r) = e^{-\beta W^{(2)}(r)}$, while according to the virial expansion [50,53] $g(r) = e^{-\beta W^{(2)}(r)} = e^{-\beta \phi(r)}$, which is valid in the low-density limit. The difference between $W^{(2)}(r)$ and $\phi(r)$ shows the influence of quantum effects and medium on the interparticle interaction.

The PMFs in Figs. 2(b1)–2(b3) are related to the discussed above RDFs in Figs. 2(a1)–2(a3). The PMFs determine the effective two-particle interaction and can be used in the mean-field theory. The depth of a PMF increases with increasing density, temperature, and hardness n , while the width of a PMF is of the order of the thermal wavelength and becomes smaller with increasing temperature. Fast oscillations are attributed to the Monte Carlo statistical error.

To estimate the possibility of arising bound states in a PMF the semiclassical Bohr-Sommerfeld condition [54] can be used for a particle in an effective spherically symmetric

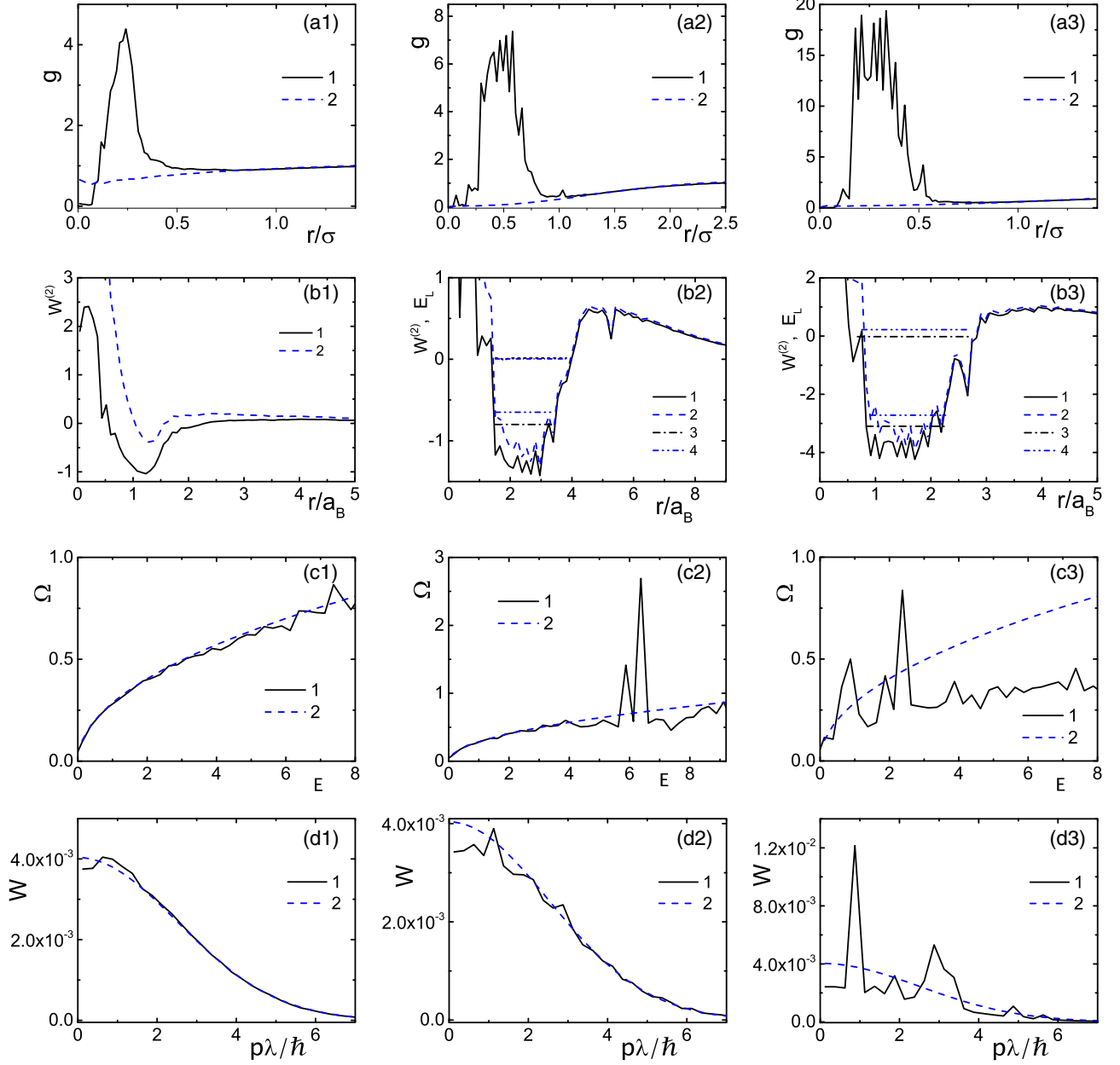


FIG. 2. The typical spin resolved RDFs [(a1)–(a3)], potentials of mean force (PMFs) as well as the averaged energy levels E_L [(b1)–(b3)], DOS [(c1)–(c3)], and momentum distribution functions MDFs [(d1)–(d3)]. Panels from the left-hand side to the right one: (left) $T = 40$ K, $r_s = 3.77$, and $n = 0.2$; (middle) $T = 20$ K, $r_s = 6.84$, and $n = 1.4$; and (right) $T = 40$ K, $r_s = 3.77$, and $n = 1.4$. Lines $g_{ab}(r)$ in panels (a1)–(a3): 1 and 2, the same and opposite spin projections, respectively. Lines $W^{(2)}(r) + \frac{L(L+1)}{2r^2}$ in panels (b1)–(b3): 1, at $L = 0$ and 2, at $L = 1$. Horizontal lines E_L in panels (b1)–(b3) at $L = 0$ and $L = 1$: 1 and 2 — $n_r = 0$; 3 and 4 — $n_r = 1$, respectively. Lines Ω in panels (c1)–(c3): 1, WPIMC; 2, ideal system. Lines $W(|p|)$ in panels (d1)–(d3): 1, WPIMC; 2, the Maxwell distribution function. Results are in conditional units. Irregular oscillations indicate the Monte Carlo statistical error.

well. The PMF is determined up to an arbitrary constant, so to agree with the virial expansion at low density we have to assume here that $W^{(2)}(r) = 0$ in the limit $r \rightarrow \infty$. So the effective Schrödinger equation for the radial part $R(r)$ of the wave function in atomic units looks like

$$-\frac{1}{2}R'' + \frac{L(L+1)}{2r^2}R - \left(\frac{k_B T}{\text{Ha}}\right) \frac{m_a}{m_e} \ln(g(r))R = \left(\frac{E_L}{\text{Ha}}\right) \frac{m_a}{m_e} R, \quad (16)$$

where E_L is the energy level, $L = 0, 1, 2, \dots$ is the orbital quantum number [54]. The Bohr-Sommerfeld condition has the form

$$\int_{r_1(E)}^{r_2(E)} p(r) dr = \pi \left(n_r + \frac{1}{2} \right), \quad (17)$$

where

$$p(r) = \sqrt{2 \left[\tilde{E} + \left(\frac{k_B T}{\text{Ha}}\right) \frac{m_a}{m_e} \ln(g(r)) \right] - \frac{(L + \frac{1}{2})^2}{r^2}}.$$

Here $\tilde{E} = (\frac{E}{\text{Ha}}) \frac{m_a}{m_e}$, m_a , and m_e are the soft-sphere and electron masses, respectively, n_r is the number of zeros of $R(r)$ [54] and for any energy $E \geq W_{\min}^{(2)}$ there are only two turning points r_1 and r_2 . Lines 1 and 2 in Figs. 2(b1)–2(b3) show the PMF $W^{(2)}(r)$ and the sum of $W^{(2)}(r)$ and $\frac{L(L+1/2)}{2r^2}$ for $L = 1$.

The energy levels of bound states obtained from the Bohr-Sommerfeld condition [54] are presented at $L = 0$ and $L = 1$ by horizontal solid lines 1 and 2 for $n_r = 0$ and by dashed lines 3 and 4 for $n_r = 1$ in Figs. 2(b1)–2(b3), respectively. The energy levels E_L are obtained according to Eq. (17). The RDFs for fermions with opposite spin projections are nonzero inside the PMF wells. As a consequence some fermions can occupy these energy levels forming a nonstable triplet cluster of two particles with the same spin and one with the opposite spin [33]. For a soft-sphere potential with $n = 0.2$, Eq. (17) cannot be satisfied under any energy E .

C. DOS and momentum distribution

Figures 2(c1)–2(c3) and Figs. 2(d1)–2(d3) demonstrate the DOS and MDFs for a strongly coupled system of soft-sphere fermions. For a very soft interparticle potential with hardness $n = 0.2$ the WPIMC DOS and MDFs are nearly classical: $\Omega \sim \sqrt{E}$ and $W(E)$ is the Maxwell-Boltzmann distribution function (see left column in Fig. 2). We also confirm the agreement of our calculations for ideal fermions with the ideal DOS and Maxwell MDF, which demonstrate the accuracy of our approach in a wide range of particle momentum, where the decay of MDF is about six orders of magnitude (not shown).

Figures 2(c1)–2(c3) and Figs. 2(d1)–2(d3) show that strong interaction results in the sharp peaks on the DOS and MDF curves. These peaks arise due to the interference of quantum effects and degeneracy introduced by the determinant in Eq. (13). As $\Omega(E)$ and $W(E)$ are normalized to unity the appearance of sharp peaks is compensated by the extended pits on both functions, which can be clearly seen in Figs. 2(c1)–2(c3) and Figs. 2(d1)–2(d3) of Fig. 2 [$\Omega(E) = \exp(E)W(E)$].

From the physical point of view, the soft-sphere repulsive interaction increases the energy of any given phase-space configuration in comparison with the same configuration of the ideal system. As the energy distribution is proportional to the fraction of phase-space states with an energy equal to E , then this fraction [$W(E)$] needs to be shifted to larger energy. As a consequence, this is also true for DOS, which we can see in Fig. 2.

Let us note that in Figs. 2(b1)–2(b3) and Figs. 2(c1)–2(c3) the energy is in “atomic units for considered soft spheres,” so it is normalized by temperature ~ 27 K [$27 = (\frac{T}{\text{Ha}}) \frac{m_a}{m_e k_B}$]. As the energy scale on the horizontal axis of the middle column ($T = 20/27$ K) is two times larger than in the left and right ones ($T = 40/27$ K), the position in the absolute energy of the double peak of the DOS in the middle column resembles practically the analogous one in the right column, which supports weak dependence of Ω on temperature. The higher density in the right column ($r_s = 3.77$) results in the appearance of the additional peaks at low energy ($E/27 \sim 1$) in comparison with the middle column ($r_s = 6.84$).

The momenta corresponding to the discussed above bound states can be estimated as the average values of momentum $\langle p(r)\lambda/\hbar \rangle$ in (17). Let us stress that the noticeable repetition

and correlation in the positions of the three peaks on the MDF in Fig. 2(d) is supported by the structure of the energy levels corresponding to the Bohr-Sommerfeld condition. The peak heights are higher for increasing temperature and density (see the middle and right columns) ($T = 20$ K, $r_s = 6.84$, and $n = 1.4$) and ($T = 40$ K, $r_s = 3.77$, and $n = 1.4$). The same tendency of increasing peak heights can be seen in Fig. 2(d) at increasing hardness from $n = 0.2$ to $n = 1.4$ and fixed values of other parameters (see left and right columns). The physical reason of this tendency is the increasing sharp variation of the characteristic spatial potential energy field and the decreasing ratio of the particle thermal wavelength to the potential field spacial landscape (due to a faster decay of singularities).

IV. DISCUSSION

Density of states is an important property that can be used to calculate thermodynamic potential and other thermodynamic functions (including entropy) of a classical or quantum system of particles. Contrary to the Wang-Landau method [4–11], which was applied to a classical system, this article deals with quantum systems. The Wigner formulation of quantum mechanics was used to derive the path-integral representation of the quantum density of states in the canonical ensemble. The WPIMC approach is able to calculate DOS, thermodynamic functions, and MDF in one simulation. The obtained MDF resembles the Maxwell-Boltzmann distribution but takes into account quantum effects.

The 3D quantum system of strongly correlated soft-sphere fermions was considered as an interesting physical example. A number of properties were calculated by the WPIMC method for different densities and temperatures, including DOS, MDFs, spin-resolved RDFs, PMFs, and related semi-classical energy levels.

The physical meaning of the sharp peaks arising on the RDFs, DOS, and MDFs has been analyzed and explained by the manifestation of the Fermi repulsion and bound states.

ACKNOWLEDGMENTS

We thank G. S. Demyanov for comments and help in numerical matters. We value stimulating discussions with Prof. M. Bonitz, T. Schoof, S. Groth, and T. Dornheim. The authors acknowledge the JIHT RAS Supercomputer Centre, the Joint Supercomputer Centre of the Russian Academy of Sciences, and the Shared Resource Centre “Far Eastern Computing Resource” IACP FEB RAS for providing computing time.

APPENDIX A: QUANTUM PSEUDOPOTENTIAL FOR SOFT-SPHERE FERMIONS

The high-temperature density matrix $\rho^{(j)} = \langle r^{(j)} | e^{-\epsilon \hat{H}} | r^{(j+1)} \rangle$ can be expressed as a product of two-particle density matrices [23],

$$\begin{aligned} \rho(r_l, r'_l, r_t, r'_t; \epsilon) &= \frac{1}{\tilde{\lambda}^6} \exp \left[-\frac{\pi}{\tilde{\lambda}^2} |r_l - r'_l|^2 \right] \\ &\times \exp \left[-\frac{\pi}{\tilde{\lambda}^2} |r_t - r'_t|^2 \right] \exp \left[-\epsilon \Phi_{lt}^{\text{OD}} \right]. \end{aligned} \quad (\text{A1})$$

This formula results from the factorization of the density matrix into the kinetic and potential parts, $\rho \approx \rho_0^K \rho^U$. The off-diagonal density matrix element (A1) involves an effective pair interaction by a pseudopotential, which can be expressed approximately via its diagonal elements, $\Phi_{li}^{\text{OD}}(r_l, r'_l, r_t, r'_t; \epsilon) \approx [\Phi_{li}(r_l - r_t; \epsilon) + \Phi_{li}(r'_l - r'_t; \epsilon)]/2$.

To estimate $\Phi(r)$ for each high-temperature density matrix we use the Kelbg functional [55,56], allowing us to take into account quantum effects in interparticle interaction. The pseudopotential $\Phi(r)$ is defined by the Fourier transform $v(t)$ of the potential $\phi(r)$. This transform can be found at $n < 3$ for the corresponding Yukawa-like potential $\exp(-\kappa r)/r^n$ in the limit of “zero screening” ($\kappa \rightarrow 0$),

$$v(t) = \frac{4\pi t^n \Gamma(2-n) \sin(n\pi/2)}{t^3}, \quad (\text{A2})$$

where Γ is the gamma function. The resulting quantum pseudopotential has the following form:

$$\begin{aligned} \Phi(r) &= \frac{\sqrt{\pi}}{8\pi^3} \int_0^\infty v(t) \exp[-(\tilde{\lambda}t)^2/4] \\ &\times \frac{\sin(tr) \text{erfi}(\tilde{\lambda}t/2)}{(tr)\tilde{\lambda}t} 4\pi t^2 dt, \end{aligned} \quad (\text{A3})$$

where $\text{erfi}(z) = i \text{erf}(iz)$, $\text{erf}(z)$ is the error function [55]. This pseudopotential is finite at zero interparticle distance $\Phi(0) = \lambda^{-n} \Gamma(1-n/2)$ and decreases according to the power law $(\lambda/r)^n$ for distances larger than the thermal wavelength.

For more accurate accounting for quantum effects the “potential energy” $U(q^j, q^{j+1})$ in (10) and (13) (see Appendix A) has to be taken as the sum of pair interactions given by Φ^{OD} with $\Phi(r)$. Pseudopotential Φ was also used in the Hamilton function $H(p, q)$ in the Weyl’s symbol of the operator $\delta(E\hat{I} - \hat{H})$ [see Eqs. (3) and (7)].

APPENDIX B: WIGNER-PATH INTEGRAL MONTE CARLO METHOD

In this article the WPIMC approach is used in the framework of approximation (13) of the Wigner function. In general, to calculate average values of any quantum operator $\langle \hat{A} \rangle$ the following representation of $\langle \hat{A} \rangle$ can be used [22–24,32]:

$$\begin{aligned} \langle \hat{A} \rangle &= \int dPdQ A(P, Q) W(P, Q) \\ &= \frac{\langle A(P, Q) \cdot h(P, Q) \rangle_{\tilde{W}}}{\langle h(P, Q) \rangle_{\tilde{W}}}, \end{aligned} \quad (\text{B1})$$

where, for example, the Weyl’s symbol of operator \hat{A} is

$$A(P, Q) = \delta[E - H(P, Q)]. \quad (\text{B2})$$

Here brackets $\langle g(P, Q) \rangle_{\tilde{W}}$ denote the averaging of any function $g(P, Q)$ with a weight $\tilde{W}(P, Q)$,

$$\langle g(P, Q) \rangle_{\tilde{W}} = \int dPdQ g(P, Q) \tilde{W}(P, Q). \quad (\text{B3})$$

To calculate the main contribution to $\langle \hat{A} \rangle$ the function $\tilde{W}(P, Q)$ can be written as the absolute value of a real part of the Wigner functions [30] and a function $h(P, Q)$ accounting for the sign of $\text{Re}(W(P, Q))$ [23,24,30],

$$h(P, Q) = \text{sgn}(\text{Re}(W(P, Q))),$$

$$\tilde{W}(P, Q) = |\text{Re}(W(P, Q))|. \quad (\text{B4})$$

Note that the partition function Z and constant $\tilde{C}(M)$ in (13) are canceled in Monte Carlo calculations.

The basic idea of a Monte Carlo method is to replace the integration in Eq. (B3) with the averaging over samples $\{\bar{\mathbf{x}}_1, \bar{\mathbf{x}}_2, \dots, \bar{\mathbf{x}}_M\}$ of a random vector $\bar{\mathbf{x}}$,

$$\langle \hat{A} \rangle = \frac{\sum_{i=1}^M A(\bar{\mathbf{x}}_i) h(\bar{\mathbf{x}}_i)}{\sum_{i=1}^M h(\bar{\mathbf{x}}_i)}, \quad (\text{B5})$$

where the random quantities $\bar{\mathbf{x}}_i \equiv (P, Q)_i$ are drawn from any distribution $\tilde{W}(\bar{\mathbf{x}})/\tilde{Q}$ ($\tilde{Q} = \int_\Omega \tilde{W}(\bar{\mathbf{x}}) d\bar{\mathbf{x}}$). According to the law of large numbers, if random vectors $\bar{\mathbf{x}}_i$ are not correlated, then the statistical error is proportional to $1/\sqrt{M}$ and can be estimated using the 3σ rule. If $h(\bar{\mathbf{x}}_i) \equiv 1$, then this expression gives the usual average value.

The samples $\{\bar{\mathbf{x}}_1, \bar{\mathbf{x}}_2, \dots, \bar{\mathbf{x}}_M\}$ of a random vector $\bar{\mathbf{x}}$ with a probability density $\tilde{W}(\bar{\mathbf{x}})$ can be obtained using the Metropolis algorithm. The Metropolis algorithm is based on the Markov process, which can be constructed by using the transition probabilities. This algorithm consists of sequential steps divided into two substeps: proposal and acceptance. Suppose the system is in a state $\bar{\mathbf{x}}_i$, i.e., the random vector $\bar{\mathbf{x}}$ has a value $\bar{\mathbf{x}}_i$. On the proposal step a new random vector $\bar{\mathbf{x}}'_i$ is generated. On the acceptance step this new state can be accepted with a probability $A(\bar{\mathbf{x}}_i \rightarrow \bar{\mathbf{x}}'_i)$, and then $\bar{\mathbf{x}}_{i+1} = \bar{\mathbf{x}}'_i$, or rejected, and then $\bar{\mathbf{x}}_{i+1} = \bar{\mathbf{x}}_i$. The acceptance probability $A(\bar{\mathbf{x}}_i \rightarrow \bar{\mathbf{x}}'_i)$ must be set to satisfy the detailed balance equation, and the most common choice is

$$A(\bar{\mathbf{x}}_i \rightarrow \bar{\mathbf{x}}'_i) = \min\left(1, \frac{\tilde{W}(\bar{\mathbf{x}}'_i)}{\tilde{W}(\bar{\mathbf{x}}_i)}\right). \quad (\text{B6})$$

The arising stationary distribution of $\{\bar{\mathbf{x}}_i\}$ has to be equal to $\tilde{W}(\bar{\mathbf{x}})$.

- [1] H. Shimizu, *Phys. Rev. E* **70**, 056704 (2004).
- [2] M. Habeck, *Phys. Rev. Lett.* **98**, 200601 (2007).
- [3] A. Montecinos, C. Loyola, J. Peralta, and S. Davis, *Physica A* **562**, 125279 (2021).
- [4] F. Wang and D. P. Landau, *Phys. Rev. E* **64**, 056101 (2001).
- [5] F. Wang and D. P. Landau, *Phys. Rev. Lett.* **86**, 2050 (2001).
- [6] R. Faller and J. J. de Pablo, *J. Chem. Phys.* **119**, 4405 (2003).

- [7] T. Vogel, Y. W. Li, T. Wüst, and D. P. Landau, *Phys. Rev. Lett.* **110**, 210603 (2013).
- [8] F. Liang, *J. Am. Stat. Assoc.* **100**, 1311 (2005).
- [9] F. Moreno, S. Davis, and J. Peralta, *Comput. Phys. Commun.* **274**, 108283 (2022).
- [10] L. Bornn, P. E. Jacob, P. Del Moral, and A. Doucet, *J. Comput. Graph. Stat.* **22**, 749 (2013).

- [11] Y. F. Atchadé and J. S. Liu, *Stat. Sinica* **20**, 209 (2010).
- [12] M. Probert, *Contemporary Phys.* **52**, 77 (2011).
- [13] D.-H. Seo, H. Shin, K. Kang, H. Kim, and S. S. Han, *J. Phys. Chem. Lett.* **5**, 1819 (2014).
- [14] X. Ma, Z. Li, L. E. Achenie, and H. Xin, *J. Phys. Chem. Lett.* **6**, 3528 (2015).
- [15] L. E. Ratcliff, S. Mohr, G. Huhs, T. Deutsch, M. Masella, and L. Genovese, *WIREs Comput. Mol. Sci.* **7**, e1290 (2017).
- [16] G. Galli, *Curr. Opin. Solid State Mater. Sci.* **1**, 864 (1996).
- [17] Y. Saad, J. R. Chelikowsky, and S. M. Shontz, *SIAM Rev.* **52**, 3 (2010).
- [18] S. Goedecker, *Rev. Mod. Phys.* **71**, 1085 (1999).
- [19] P. Vorontsov-Velyaminov and A. Lyubartsev, *J. Phys. A: Math. Gen.* **36**, 685 (2003).
- [20] J. Lee, *Phys. Rev. Lett.* **71**, 211 (1993).
- [21] R. P. Feynman and A. R. Hibbs, *Quantum Mechanics and Path Integrals* (McGraw-Hill, New York, 1965).
- [22] V. Zamalin, G. Norman, and V. Filinov, *The Monte Carlo Method in Statistical Thermodynamics* (Nauka, Moscow, 1977).
- [23] W. Ebeling, V. Fortov, and V. Filinov, *Quantum Statistics of Dense Gases and Nonideal Plasmas* (Springer, Berlin, 2017).
- [24] V. Fortov, V. Filinov, A. Larkin, and W. Ebeling, *Statistical Physics of Dense Gases and Nonideal Plasmas* (PhysMatLit, Moscow, 2020).
- [25] J. Runeson, M. Nava, and M. Parrinello, *Phys. Rev. Lett.* **121**, 140602 (2018).
- [26] T. Dornheim, M. Invernizzi, J. Vorberger, and B. Hirshberg, *J. Chem. Phys.* **153**, 234104 (2020).
- [27] D. M. Ceperley, *J. Stat. Phys.* **63**, 1237 (1991).
- [28] D. M. Ceperley, *Phys. Rev. Lett.* **69**, 331 (1992).
- [29] E. Wigner, *Phys. Rev.* **46**, 1002 (1934).
- [30] V. I. Tatarskii, *Sov. Phys. Usp.* **26**, 311 (1983).
- [31] A. Larkin, V. Filinov, and V. Fortov, *Contrib. Plasma Phys.* **57**, 506 (2017).
- [32] A. Larkin, V. Filinov, and V. Fortov, *J. Phys. A: Math. Theor.* **51**, 035002 (2018).
- [33] V. Filinov, P. Levashov, and A. Larkin, [arXiv:2305.07601](https://arxiv.org/abs/2305.07601).
- [34] W. H. Miller and S. J. Cotton, *J. Chem. Phys.* **145**, 081102 (2016).
- [35] S. J. Cotton and W. H. Miller, *J. Chem. Theory Comput.* **12**, 983 (2016).
- [36] S. J. Cotton and W. H. Miller, *J. Phys. Chem. A* **119**, 12138 (2015).
- [37] W. Luyten, *J. R. Astron. Soc. Can.* **65**, 304 (1971).
- [38] A. Y. Potekhin, *Phys. Usp.* **53**, 1235 (2011).
- [39] T. Dornheim, S. Groth, and M. Bonitz, *Phys. Rep.* **744**, 1 (2018).
- [40] D. M. Ceperley, *Rev. Mod. Phys.* **67**, 279 (1995).
- [41] R. Kubo, M. Toda, and N. Hashitsume, *Statistical Physics II: Nonequilibrium Statistical Mechanics* (Springer Science & Business Media, New York, 2012), Vol. 31.
- [42] L. M. Sesé, *Entropy* **22**, 1338 (2020).
- [43] V. Filinov, R. Syrovatka, and P. Levashov, *Mol. Phys.* **120**, e2102549 (2022).
- [44] V. Zamalin and G. Norman, *USSR Comput. Math. Math. Phys.* **13**, 169 (1973).
- [45] A. Larkin, V. Filinov, and V. Fortov, *Contrib. Plasma Phys.* **56**, 187 (2016).
- [46] V. Filinov, A. Larkin, and P. Levashov, *Universe* **8**, 79 (2022).
- [47] V. S. Filinov, A. S. Larkin, and P. R. Levashov, *Phys. Rev. E* **102**, 033203 (2020).
- [48] V. Filinov, P. Levashov, and A. Larkin, *J. Phys. A: Math. Theor.* **55**, 035001 (2022).
- [49] J. G. Kirkwood, *J. Chem. Phys.* **3**, 300 (1935).
- [50] I. Z. Fisher, *Statistical Theory of Liquids* (University of Chicago Press, Chicago, 1964).
- [51] J. Barker and D. Henderson, *Annu. Rev. Phys. Chem.* **23**, 439 (1972).
- [52] J. G. Kirkwood, E. K. Maun, and B. J. Alder, *J. Chem. Phys.* **18**, 1040 (1950).
- [53] B. Zelener, G. Norman, and V. Filinov, *Perturbation Theory and Pseudopotential in Statistical Thermodynamics* (Nauka, Moscow, 1981).
- [54] A. F. Nikiforov, V. G. Novikov, and V. B. Uvarov, *Quantum-Statistical Models of Hot Dense Matter: Methods for Computation Opacity and Equation of State* (Springer Science & Business Media, New York, 2005), Vol. 37.
- [55] G. Demyanov and P. Levashov, [arXiv:2205.09885](https://arxiv.org/abs/2205.09885).
- [56] G. Kelbg, *Ann. Phys.* **467**, 354 (1963).